



UNIVERSIDAD POLITÉCNICA DE MADRID

ESCUELA TÉCNICA SUPERIOR DE INGENIEROS AERONÁUTICOS



BETsMA Manual

Dr. G. Sánchez-Arriaga

Departamento de Física Aplicada

April 9, 2014

CONTENTS

0.1	About BETsMA	1
0.2	Getting started	3
0.3	Tether system configuration	7
0.4	Physical models	8
0.4.1	Deorbiting model	8
0.4.1.1	Coordinate and time systems	8
0.4.1.2	Equation of motion	9
0.4.1.3	The circular deorbiting model	10
0.4.1.4	The <i>non-averaged</i> deorbiting model	11
0.4.2	Environment models	12
0.4.2.1	Geomagnetic field models	12
0.4.2.2	Plasma density model	13
0.4.2.3	Air density model	14
0.4.3	Current collection model	14
0.4.3.1	Current and voltages profiles	14
0.4.4	Tether survivability model	18
0.4.5	Growth rate of the dynamical instability and self-balanced tether	19
0.4.6	Mass estimation of the tether subsystems	21
0.5	Optimization method in tape-tether design	22
0.6	BETsMA Interface	23
0.6.1	The <i>main</i> windows	23

0.6.2	The <i>control</i> window	24
0.6.2.1	The optimization module	24
0.6.2.2	The deorbiting module	26
0.7	Validation of the code	31
0.7.1	Tether current collection model	31
0.7.2	Tether survival probability	32
0.7.3	Orbital propagator	32
0.7.4	Global check of the deorbiting module	34
0.8	Preliminary mission design example	35
0.8.1	Tether optimal geometry	35
0.8.2	Deorbiting mission performance	38
.1	BETsMA constants	42

0.1 About BETsMA

BETsMA is a program developed under the European Commission FP7 Space Project *Propellantless deorbiting of space debris by bare electrodynamic tethers* (Project Acronym: BETs, number: 262972 and duration 1/11/2010-31/1/2014). It is dedicated to preliminary analysis of deorbiting missions with bare electrodynamic tethers. The software has two modules:

1. Optimization module. Given a mission (altitude, inclination and satellite mass), the program computes certain figures of merit of the tether system as a function of the tether geometry (length, width and thickness). Using this module, the user can find the optimal tether geometry to minimize the mass of the system, the deorbit time and the cut probability.
2. Deorbiting module. Given a mission and a tether system, BETsMA computes the deorbiting maneuver using a simple model based on a rigid dumbbell tether aligned with the local vertical. The program provides the most relevant magnitudes, including trajectory, deorbit time, cut probability, mass of the subsystems, electrical variables and plasma environmental magnitudes.

Both parts complement each other and give preliminary parameters of deorbiting mission with bare tethers. BETsMA's goals include a first estimation of the performances of the system and its cost in term of mass. For an specific mission, this analysis should be continued with more detailed simulations of the tether.

The code was developed at ETSI Aeronáuticos (Universidad Politécnica de Madrid) by Dr. G. Sánchez-Arriaga. Professor J. Sanmartín (BETs Coordinator) invented the *optimal design* algorithm and Mr. S. B. Khan, and Dr. A. Sánchez-Torres contributed to its development. Three BETs partners, EMXYS, DLR and Colorado State University provided the scaling laws to estimate the mass of the power system, the tether deployer and the hollow cathode, respectively.

The code is based on the results of a set of scholar papers. The most important are:

1. Sanmartin, J. R., Martínez-Sánchez, M., and Ahedo, E., *Bare Wire Anodes for Electrodynamic Tethers*, J. of Propulsion and Power 9, 353, 1993.
2. Sanmartin, J. R., and Estes, R. D., *The orbital-motion-limited regime of cylindrical Langmuir probes*, Physics of Plasmas, 6,1, 1999.
3. Khan, S. B., and Sanmartín, J. R., *Comparison of probability of survival for round and tape tethers against debris impact*, J. of Spacecraft and Rockets (to be published).
4. Sanmartín, J. R., Sánchez-Torres A., Sánchez-Arriaga, G. and Charro, M., *Optimization of tape-tether lengths for de-orbiting satellites at end of mission*, (to be submitted).

BETsMA uses the following libraries/programs not developed by the authors:

1. The fortran program *igrf11_syn.f90* is used to compute the geomagnetic field.
2. IRI 2012, an international project sponsored by the Committee on Space Research (COSPAR) and the International Union of Radio Science (URSI), is used to compute ionospheric plasma properties. License can be found at <http://irimodel.org/IRI-2012/>.
3. DISLIN is a free for non-commercial use high-level plotting library developed at the Max Plack Institute. Full BETsMA version can be distributed with and without DISLIN. If DISLIN is included, a license must be requested at <http://www.dislin.de/>.

The authors acknowledge Dr. S. Macmillan and Dr. D. Bilitza for their help with *igrf11_syn.f90* and IRI 2012, respectively. Dr. G. Sánchez-Arriaga thanks Dr. C. Bombardelli and Prof. J. Peláez for their help validating BETsMA and the implementation of the orbit propagator DROMO [9].

Contact and web page:

1. gonzalo.sanchez@upm.es
2. <http://www.thebetsproject.com/>

0.2 Getting started

BETsMA is a Fortran90 program that runs under Windows XP and Windows 7. There are two versions:

1. BETsMA Share Version. The file BETsMA_Share.msi, can be freely downloaded from the web page:

<http://www.thebetsproject.com/>

This non-commercial version is valid for orbit inclination and satellite mass below 20° and 100kg, respectively. It is installed by executing the file and following the instructions of the screen. After the installation has been finished, **the user must give permissions to write and read files inside the BETsMA folder**. This must be done manually by clicking the folder BETsMA with the right button of the mouse, *properties* – > *security*.

2. BETsMA Full Version. BETsMA is a licensed code that belong to Universidad Politécnica de Madrid. Interested users can ask for a license of the code to

gonzalo.sanchez@upm.es

This version has no limitation and can be used in a broad range of orbit and satellite conditions. The file BETsMA.msi and a code number will be sent to the user after the licensed has been obtained. This version is installed by executing the file and following the instructions of the screen. The code number must be provided during the installation. After finishing, **the user must give permissions to write and read files inside the BETsMA folder**. This must be done manually by clicking the folder BETsMA with the right button of the mouse, *properties* – > *security*.

NOMENCLATURE

IJK = Geocentric equatorial inertial (GEI) frame axis

$\hat{I}\hat{J}\hat{K}$ = International Terrestrial Reference frame (ITRF) axis

PQW = Perifocal Coordinate System

RSW = Satellite Coordinate System axis

α = Right ascension angles

δ = Latitude or space debris diameter

ΔV_{HC} = Hollow Cathode potential drop

ϵ_i = Dimensionless parameter controlling the tether instability

Γ = Tether dynamical instability growth rate

λ = longitude

$\lambda_{De}, \lambda_{Di}$ = Electron, ion Debye lengths

μ = Earth standard gravitational parameter

ν = Orbit true anomaly

ω = Orbit perigee argument

ω_{\oplus} = Earth angular velocity

Ω = Orbit longitude of ascending node

ϕ_d = Magnetic dipole longitude angle

ϕ_{lon} = East longitude angle

$\Phi(x)$ = Potential bias distribution along the tether

ρ_{air} = Air density

σ = Tether conductivity

θ_{col} = Colatitude angle

θ_d = Magnetic dipole colatitude angle

θ_{GMST} = Greenwich Mean Sidereal Time

A = Conductive tether cross section

$A_{satellite}^f$ = Satellite frontal area

A_{tether}^f = Tether frontal area

a = Orbit semimajor axis

\mathbf{a}_p = Perturbation force/ M_S

\mathbf{B} = Geomagnetic field

C_D = Drag coefficient

e = Orbit eccentricity

E_m = Motional electric field along the tether direction

f_e = Dimensionless Lorentz torque factor

h = Conductive tether thickness

h_i = Inert tether thickness

i = Orbit inclination

$I(x)$ = Current distribution along the tether

I_{av} = Averaged current along the tether

i_{av} = Normalized current along the tether

I_G = Conductive and inert tether moment of inertia about the center of mass.

L^* = Tether characteristic length

L = Conductive tether length

L_i = Inert tether length

m_c = Conductive tether mass

m_{deploy} = Deployer mass

m_{HC} = Hollow Cathode mass

m_i = Inert tether mass

m_{power} = Power subsystem mass

M_s = Satellite mass

M_T = Total mass

\dot{n}_c = Fatal impact rate per unit length

N_0 = Plasma density

N_c = Cut probability

p = Conductive tether perimeter

\mathbf{r}_s = Satellite position vector

T_e, T_i = Electron, ion temperatures

\mathbf{u}_t = Unit vector along the tether point in the direction of the electric field

\mathbf{v}_s = Satellite velocity vector

\mathbf{v}_{pl} = Plasma velocity vector

\mathbf{v}_{rel} = Tether-to-plasma (or air) relative velocity vector

w = Conductive tether width

w_i = Inert tether width

0.3 Tether system configuration

BETsMA considers a tether system made of:

1. Conductive tether segment (mass m_c , length L , width w and thickness h).
2. Inert tether segment (mass m_i , length L_i , width w_i and thickness h_i).
3. Power system (mass m_{power}).
4. Deployer system (mass m_{deploy}).
5. Plasma contactor of type hollow cathode (mass m_{HC}).

The configuration of the full tether system depend on the specific mission and may be designed carefully. However, most of the results of BETsMA are independent of this issue and they are just controlled by the properties of the conductive tether segment. An exception is the growth rate of the dynamical instability, which is severely affected by the tether system configuration.

Figure 1 shows the tether system configuration considered by BETsMA. The conductive bare tether is attached to a spacecraft of mass M_s and followed by an inert (non conductive) tether that connects to the end mass. The Hollow Cathode is at the spacecraft and the deployer is used as a tip mass. For prograde (retrograde) orbits the tether system is deployed upwards (downwards).

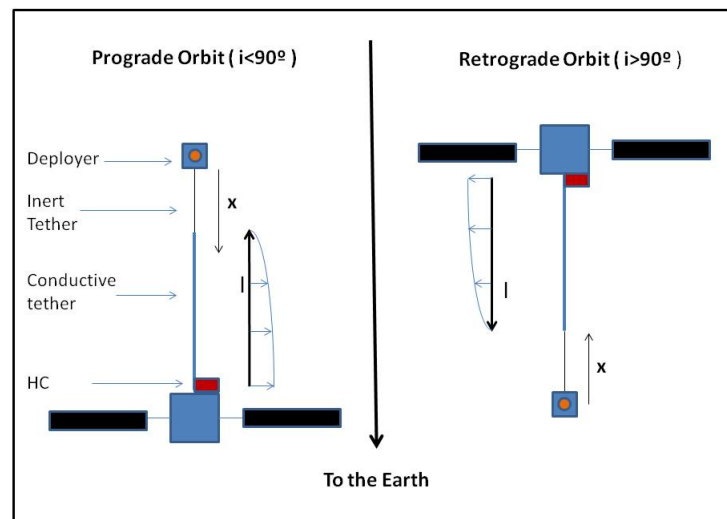


Figure 1: Tether system configuration in prograde and retrograde orbits.

0.4 Physical models

0.4.1 Deorbiting model

0.4.1.1 Coordinate and time systems

BETsMA uses four reference systems:

1. *Geocentric equatorial inertial frame* (GEI) [\mathbf{IJK}]. This system has its origin at the center of the Earth and its fundamental plane is the Earth's equator. The I axis points towards the vernal equinox, the J axis is 90° to the east in the equatorial plane and K is along the North Pole. This system is taken as an inertial frame.
2. *International Terrestrial Reference frame* (ITRF) [$\hat{\mathbf{I}}\hat{\mathbf{J}}\hat{\mathbf{K}}$]. This system is fixed to the rotating Earth, has its origin at the center of the Earth and its fundamental plane is the Earth's equator. The \hat{I} axis points towards the Greenwich meridian, the \hat{J} axis is 90° to the east in the equatorial plane and \hat{K} is along the North Pole.
3. *Satellite Coordinate System* (RSW) [\mathbf{RSW}]. This system moves with the satellite and it has the R axis always pointing from the Earth's center along the radius vector \mathbf{r}_s toward the satellite. The S axis is perpendicular to R and belong to the plane spanned by R and the satellite velocity vector \mathbf{v}_s . The W axis is normal to the orbital plane.
4. *Perifocal Coordinate System* (PCS) [\mathbf{PQW}]. This system has its origin at the Earth's center, P axis is along the periapsis of the instantaneous satellite orbit, Q is normal to P and contained in the orbital plane (defined by the \mathbf{r}_s and \mathbf{v}_s vectors). The W axis is normal to the orbital plane.

Given the six orbital elements and time it is possible to find the position \mathbf{r}_s and velocity \mathbf{v}_s vectors of the satellite. In the Perifocal Coordinate System one finds

$$\mathbf{r}_s^{PQW} = \left[\frac{p \cos \nu}{1 + e \cos \nu}, \frac{p \sin \nu}{1 + e \cos \nu}, 0 \right]^T \quad \mathbf{v}_s^{PQW} = \left[-\sqrt{\frac{\mu}{p}} \sin \nu, \sqrt{\frac{\mu}{p}} (e + \cos \nu), 0 \right]^T \quad (1)$$

where $p = a(1 - e^2)$ is the semiparameter. In the GEI system these two vectors are given by

$$\mathbf{r}_s^{GEI}(a, e, i, \Omega, \omega, \nu) = R \mathbf{r}_s^{PQW} \quad \mathbf{v}_s^{GEI}(a, e, i, \Omega, \omega, \nu) = R \mathbf{v}_s^{PQW} \quad (2)$$

where

$$R = \begin{bmatrix} \cos \Omega \cos \omega - \sin \Omega \sin \omega \cos i & -\cos \Omega \sin \omega - \sin \Omega \cos \omega \cos i & \sin \Omega \sin i \\ \sin \Omega \cos \omega + \cos \Omega \sin \omega \cos i & -\sin \Omega \sin \omega + \cos \Omega \cos \omega \cos i & -\cos \Omega \sin i \\ \sin \omega \sin i & \cos \omega \sin i & \cos i \end{bmatrix} \quad (3)$$

Some environment subroutines involve the longitude λ and the latitude δ in the ITRF frame. Once we know the position vector in the GEI frame $\mathbf{r}_s^{GEI} = (x_{GEI}, y_{GEI}, z_{GEI})$, these two angles are computed from the following formulas

$$\lambda = \alpha - \theta_{GMST}, \quad \delta = \frac{z_{GEI}}{\sqrt{x_{GEI}^2 + y_{GEI}^2 + z_{GEI}^2}} \quad (4)$$

where θ_{GMST} (Greenwich Mean Sidereal Time) is the angle between the vernal equinox and the Greenwich meridian. The right ascension angle α is found from the sine and cosine expressions

$$\sin \alpha = \frac{y_{GEI}}{\sqrt{x_{GEI}^2 + y_{GEI}^2}}, \quad \cos \alpha = \frac{x_{GEI}}{\sqrt{x_{GEI}^2 + y_{GEI}^2}} \quad (5)$$

0.4.1.2 Equation of motion

The equation of motion for a satellite of mass M_S orbiting around the Earth is

$$\frac{d^2 \mathbf{r}_s}{dt^2} = -\frac{\mu}{r^3} \mathbf{r} + \mathbf{a}_p \quad (6)$$

where $\mu = GM_E$. Here $\mathbf{a}_p \equiv \mathbf{F}_p/M_S$ is the acceleration due to the perturbation forces \mathbf{F}_p acting on the satellite. For instance \mathbf{F}_p includes the electromagnetic force on the tether, the air drag or the perturbation force due to the Earth's oblateness defined by the J_2 term.

BETsMA integrates Eq. 6 in two different ways. The first one, which is restricted to circular orbits, only takes into account the variation of the satellite altitude along the deorbiting and ignores changes in other orbital elements. The second integrator numerically solves Eq. 6 using the DROMO propagator [9].

Electrodynamic force. The simulator considers a rigid dumbbell tether with length, width, thickness and conductivity L , w , h and σ . Assuming a tether carrying the averaged current I_{av} and perfectly aligned with the orbit local vertical, we have

$$\mathbf{F}_{elec} = I_{av} L (\mathbf{u}_t \times \mathbf{B}) \quad (7)$$

where \mathbf{u}_t is the tangent unit vector along the tether pointing in the direction of the electric current. For deorbiting missions we require $\mathbf{F} \cdot \mathbf{v}_s < 0$ and the motional electric field

$$E_m = \mathbf{u}_t \cdot [(\mathbf{v}_s - \mathbf{v}_{pl}) \times \mathbf{B}] \quad (8)$$

should be positive. For an eastward (westward) low-inclination orbit this implies the current to flow up (down) to the tether and $\mathbf{u}_t = \mathbf{r}_s/r_s$ ($\mathbf{u}_t = -\mathbf{r}_s/r_s$). For a corotating plasma one has $\mathbf{v}_{pl} = \boldsymbol{\omega}_{\oplus} \times \mathbf{r}_s$, where $\boldsymbol{\omega}_{\oplus} = 7.2921 \times 10^{-5} \text{rad/s} \mathbf{K}$. One finds

$$\mathbf{a}_{elec} = \frac{L E_m \sigma w h}{M_S} i_{av} (\mathbf{u}_t \times \mathbf{B}) \quad (9)$$

where we introduced the averaged current normalized with the short-circuit current $i_{av} = I_{av}/E_m \sigma w h$.

Air drag. The air drag on the tether is given approximately by

$$\mathbf{F}_{drag} = -\frac{1}{2}\rho_{air} \left(A_{tether}^f + A_{satellite}^f \right) C_D v_{rel} \mathbf{v}_{rel} \quad (10)$$

where ρ_{air} is given by the CIRA-2012 model, \mathbf{v}_{ref} is the relative velocity between the atmosphere and the satellite, $C_D = 2.2$ is the drag coefficient, and A_{tether}^f and $A_{satellite}^f$ are the frontal area of the tether and the satellite, respectively. The relative velocity is given by

$$\mathbf{v}_{rel} = \mathbf{v}_s - \mathbf{v}_{atm}, \quad \mathbf{v}_{atm} = \boldsymbol{\omega}_{\oplus} \times \mathbf{r}_s \quad (11)$$

Using a satellite frontal area to mass ratio equal to $A_{satellite}^f/M_S = 0.01m^2/kg$ and a tether frontal area $A_{tether}^f = 2wL/\pi$ yields

$$\mathbf{a}_{drag} = -\frac{1}{2}\rho_{air} C_D \left(0.01 + \frac{2wL}{\pi M_S} \right) v_{rel} \mathbf{v}_{rel} \quad (12)$$

Earth's oblateness. The perturbation force due to Earth's oblateness is modeled by the J_2 zonal harmonic. In the GEI system one finds

$$\mathbf{a}_{J_2} = \mu J_2 \frac{R_E^2}{r_s^7} \begin{pmatrix} x \left[6z^2 - \frac{3}{2}(x^2 + y^2) \right] \\ y \left[6z^2 - \frac{3}{2}(x^2 + y^2) \right] \\ z \left[3z^2 - \frac{9}{2}(x^2 + y^2) \right] \end{pmatrix} \quad (13)$$

where $J_2 = 1.08265 \times 10^{-3}$

0.4.1.3 The circular deorbiting model

The circular deorbiting model can be used to find a quick answer about the performance of the tether system. This approximation is only valid for orbits with a small eccentricity because it assumes an initial circular orbit that evolves in a quasi-circular manner. Making the scalar product of equation 6 and \mathbf{v}_s gives

$$\frac{d}{dt} \left(\frac{1}{2} v_s^2 \right) = \frac{d}{dt} \left(\frac{\mu}{r_s} \right) + \frac{LE_m \sigma w h}{M_S} i_{av} \mathbf{v}_s \cdot (\mathbf{u}_t \times \mathbf{B}) \quad (14)$$

or, using the definition of the motional electric field,

$$\frac{d}{dt} \left(\frac{1}{2} v_s^2 \right) = \frac{d}{dt} \left(\frac{\mu}{r_s} \right) - \frac{LE_m^2 \sigma w h}{M_S} i_{av} \quad (15)$$

Making $e = 0$ in Eq. 1, we find $v_s^2 \approx \mu/r$ and substituting in Eq. 15 yields

$$\frac{dr_s}{dt} = G(\mathbf{r}_s, \mathbf{v}_s, t) \quad G(\mathbf{r}_s, \mathbf{v}_s, t) \equiv -2 \frac{L \sigma w h E_m^2}{\mu M_S} i_{av} r_s^2 \quad (16)$$

Due to the perturbations, all the orbital elements depend on time. For this simple model, however, we will assumed that they are all constant except the semimajor axis and the true anomaly which is governed by

$$\frac{d\nu}{dt} = \sqrt{\frac{\mu}{r_s^3}} \quad (17)$$

The two ordinary differential equations 16 and 17 (complemented with Eq. 2) can be integrated numerically to find the deorbiting trajectory. For the BETsMA *circular model*, however, we will make a last assumption that allows to increase the integration speed. For each radial position r_s and the initial epoch of the integration t_0 , the function $G(\mathbf{r}_s, \mathbf{v}_s, t)$ is averaged over several orbits to construct the following function

$$G_{av}(r_s) = \frac{1}{2\pi} \int_0^{2\pi} G(\mathbf{r}_s, \mathbf{v}_s, t) d\nu \quad (18)$$

The BETsMA *circular model* is then given by Eq. 17 and

$$\frac{dH}{dt} = G_{av}(H) \quad (19)$$

where $r_s = R_E + H$. At the beginning of the simulation BETsMA computes a table with G_{av} for 98 altitudes. The integral in Eq. 18 is carried out by discretizing the interval $0 - 2\pi$ with 500 points. A table with the function G_{av} versus r_s is then obtained. After this computation, the program calls to the integrator, which finds the value of $G_{av}(r_s)$ by making a linear interpolation.

0.4.1.4 The *non-averaged* deorbiting model

BETsMA carries out the numerical integration of Eq. 6 by using the orbit propagator DROMO [9, 2], which was developed at the SDG-UPM (former *Grupo de Dinámica de Tethers*). It implements a special perturbation method of variation of parameters (VOP) based on a set of redundant variables. In words of the authors [17]:

The aim of the project was to develop a regular, robust and efficient propagator. Robust means that it should be numerically stable. Efficient means that the propagator should render accurate results with low time-consumption and share a common formulation for elliptical, parabolic and hyperbolic problems. How accurate the results are and how quick the propagator provide them constitute a metric of its performance.

DROMO uses the variables $L_c \equiv |\mathbf{r}_s(0)|$ and $\omega_c \equiv \sqrt{\mu/L_c^3}$ to construct the dimensionless time $\tau \equiv \omega_c t$, position $\tilde{\mathbf{r}} \equiv \mathbf{r}_s/L_c$ and velocity $\tilde{\mathbf{v}} \equiv \mathbf{v}/L_c\omega_c$ vectors. Equation 6 then becomes

$$\frac{d^2\tilde{\mathbf{r}}}{d\tau^2} = -\frac{\tilde{\mathbf{r}}}{\tilde{r}^3} + \mathbf{a}(\tilde{\mathbf{r}}, \tilde{\mathbf{v}}, \tau), \quad \mathbf{a} \equiv \frac{a_p}{L_c\omega_c^2} \quad (20)$$

and, after introducing the redundant variables $[\sigma, \tau, \zeta_1, \zeta_2, \zeta_3, \eta_1, \eta_2, \eta_3, \eta_4]$, one finds the following set of first order differential equations

$$\frac{d\tau}{d\sigma} = \frac{1}{\zeta_3^3 s^2} \quad (21)$$

$$\frac{d\zeta_1}{d\sigma} = +s\tilde{a}_x \sin \sigma + \tilde{a}_y (\zeta_1 + \tilde{s} \cos \sigma) \quad (22)$$

$$\frac{d\zeta_2}{d\sigma} = -s\tilde{a}_x \cos \sigma + \tilde{a}_y (\zeta_2 + \tilde{s} \sin \sigma) \quad (23)$$

$$\frac{d\zeta_3}{d\sigma} = -\tilde{a}_y \zeta_3 \quad (24)$$

$$\frac{d\eta_1}{d\sigma} = +\frac{1}{2}\tilde{a}_z (\eta_4 \cos \sigma - \eta_3 \sin \sigma) \quad (25)$$

$$\frac{d\eta_2}{d\sigma} = +\frac{1}{2}\tilde{a}_z (\eta_3 \cos \sigma + \eta_4 \sin \sigma) \quad (26)$$

$$\frac{d\eta_3}{d\sigma} = -\frac{1}{2}\tilde{a}_z (\eta_2 \cos \sigma - \eta_1 \sin \sigma) \quad (27)$$

$$\frac{d\eta_4}{d\sigma} = -\frac{1}{2}\tilde{a}_z (\eta_1 \cos \sigma + \eta_2 \sin \sigma) \quad (28)$$

where

$$s = 1 + \zeta_1 \cos \sigma + \zeta_2 \sin \sigma, \quad \tilde{s} = 1 + s, \quad \tilde{a}_{x,y,z} = \frac{a_{x,y,z}}{s^3 \zeta_3^4} \quad (29)$$

Reference [17] provides explicit relations between the state vector variables $(\tilde{\mathbf{r}}, \tilde{\mathbf{v}})$ and DROMO variables $[\sigma, \tau, \zeta_1, \zeta_2, \zeta_3, \eta_1, \eta_2, \eta_3, \eta_4]$.

0.4.2 Environment models

0.4.2.1 Geomagnetic field models

BETsMA implements three magnetic field models. For convenience the magnetic field is computed in the ITRF system, which is attached to the rotating Earth. Here θ_{col} and ϕ_{long} are the colatitude and the east longitude, respectively. The models are given by

1. Dipole model. The magnetic field is given by

$$\mathbf{B}_{ITRF} = -B_{eq} \left(\frac{R_E}{r_s} \right)^3 (2 \cos \theta_{col} \mathbf{u}_r + \sin \theta_{col} \mathbf{u}_{\theta_{col}}) \quad (30)$$

where R_E is the Earth radius, B_{eq} the mean value of the magnetic field at the equator, and \mathbf{u}_r and $\mathbf{u}_{\theta_{col}}$ the unit vectors along the r and θ_{col} directions.

2. Eccentric dipole[?, ?]. The magnetic field is

$$\mathbf{B}_{ITRF} = B_{eq} \left(\frac{R_E}{r_d} \right)^3 [3(\mathbf{u}_m \cdot \mathbf{u}_d) \mathbf{u}_d - \mathbf{u}_m] \quad (31)$$

where \mathbf{u}_m is the magnetic dipole unit vector. The vector position \mathbf{r}_d of the point under consideration with respect to the center of the dipole was written as $\mathbf{r}_d \equiv r_d \mathbf{u}_d$, with \mathbf{u}_d an unit vector. In the ITRF system the vector \mathbf{u}_m is given by

$$\mathbf{u}_m = (\sin \theta_d \cos \phi_d, \sin \theta_d \sin \phi_d, \cos \theta_d) \quad (32)$$

where the colatitude θ_d and the longitude ϕ_d are given by

$$\sin \theta_d = \frac{\sqrt{g_{11}^2 + h_{11}^2}}{B_{eq}}, \quad \tan \phi_d = \frac{h_{11}}{g_{11}}, \quad B_{eq} = \sqrt{g_{10}^2 + g_{11}^2 + h_{11}^2} \quad (33)$$

The vector position with respect to the dipole center is

$$\mathbf{r}_d = \mathbf{r}_s - \begin{pmatrix} \frac{L_1 - g_{11}P}{3B_{eq}^2} \\ \frac{L_2 - h_{11}P}{3B_{eq}^2} \\ \frac{L_0 - g_{10}P}{3B_{eq}^2} \end{pmatrix} R_E, \quad (34)$$

where \mathbf{r} is the position vector of the point of interest with respect to the Earth center and

$$L_0 = 2g_{10}g_{20} + \sqrt{3}(g_{11}g_{21} + h_{11}h_{21}) \quad (35)$$

$$L_1 = -g_{11}g_{20} + \sqrt{3}(g_{10}g_{21} + g_{11}g_{22} + h_{11}h_{22}) \quad (36)$$

$$L_2 = -h_{11}g_{20} + \sqrt{3}(g_{10}h_{21} - g_{22}h_{11} + g_{11}h_{22}) \quad (37)$$

$$P = \frac{L_0g_{10} + L_1g_{11} + L_2h_{11}}{4B_{eq}^2} \quad (38)$$

3. IGRF 2011 model [5]. The magnetic field is computed as $\mathbf{B}_{ITRF} = -\nabla V$ with

$$V(r, \theta_{col}, \phi_{long}, t) = a \sum_{n=1}^N \sum_{m=0}^n \left(\frac{a}{r} \right)^{n+1} [g_n^m(t) \cos m\phi_{long} + h_n^m(t) \sin m\phi_{long}] P_n^m(\cos \theta_{col}) \quad (39)$$

Here r denotes the distance from the center of the Earth in unit of km, $a = 6371.2 \text{ km}$ is the magnetic reference spherical radius, and $g_n^m(t)$ and h_n^m the Gauss coefficients.

0.4.2.2 Plasma density model

The plasma density N_0 and electron and ion temperatures are calculated using the International Reference Ionosphere *IRI2012* [3]. These data are required to compute the current collected by the bare tether. Electron and ion temperature are used if the *beyond OML* current collection model is used.

0.4.2.3 Air density model

The density ρ_{air} appearing in Eq. 12 is computed using the following formula

$$\rho_{air} = \exp(p_0 + p_1 H + p_2 H^2 + p_3 H^3) \quad (40)$$

where the p_i coefficients are found by fitting the semi-empirical COSPAR International Reference Atmosphere (CIRA-2012) model. Figure 2 shows the density versus the altitude given by CIRA-2012 and the fitting for three solar activities.

For altitudes above 900 km BETsMA sets the density equal to zero and no atmospheric drag is considered. However, just for plotting considerations, BETsMA takes the density equal to 10^{-17}kg/m^3 to avoid an internal error with the logarithm axis.

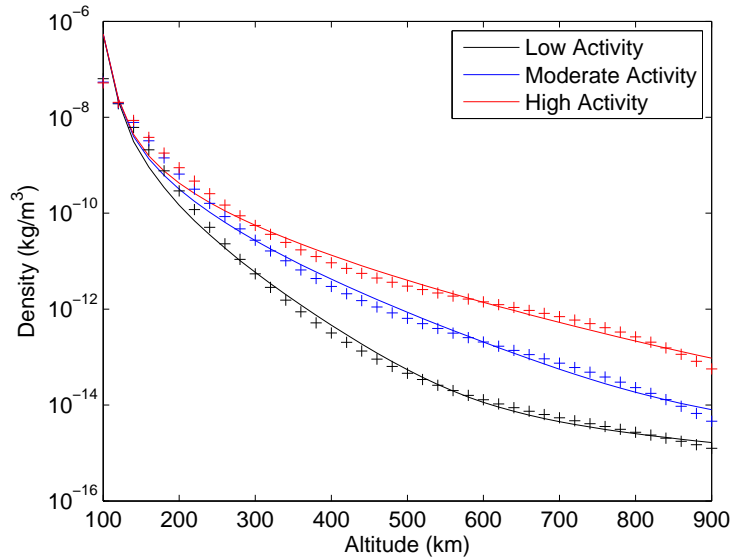


Figure 2: Air density given by CIRA-2012.

0.4.3 Current collection model

0.4.3.1 Current and voltages profiles

We consider a rigid and fully bare tether of length L , cross section area A and perimeter p made of a conductive material of density ρ and conductivity σ . Due to the plasma-to-tether relative velocity \mathbf{v}_{rel} and the ambient magnetic field \mathbf{B} , an induced electric field along the tether $E_m = \mathbf{u}_t \cdot (\mathbf{v}_{rel} \times \mathbf{B})$ appears, where \mathbf{u}_t is the tangent unit vector along the tether pointing in the direction of the electric current. The spatial variation of the plasma potential Φ_p (in the tether frame) is given by the motional electric field projected along

the tether E_m while that of the tether potential Φ_t is due to ohmic loss. The potential bias $\Phi = \Phi_t - \Phi_p$ is given by [14, 16]

$$\frac{d\Phi}{dx} = \frac{I(x)}{A\sigma} - E_m \quad (41)$$

where $I(x)$ is the intensity along the tether and $0 < x < L$.

For a bare tether, electrons are collected along the anodic length $0 < x < L_{AB}$ where $\Phi > 0$ and they are ejected by some plasma contactor (e.g. a hollow-cathode or a thermionic emitter device), at a cost of a potential drop ΔV_{HC} . The length L_{AB} , which is determined by the condition $\Phi_B = 0$, depends on the plasma conditions and must be found as part of the solution of the problem.

Since tether length L is much larger than its transverse dimension, two-dimensional plasma probe theory gives us the following equation describing the current profile in an anodic segment of perimeter p_t

$$\frac{dI(x)}{dx} = G \left(\frac{e\Phi(x)}{kT_i}, \frac{T_e}{T_i}, \frac{R}{\lambda_{Di}} \right) \times e N_0 \frac{p}{\pi} \sqrt{\frac{2e\Phi(x)}{m_e}} \quad 0 < x < L_{AB} \quad (42)$$

The right hand side of the above equation is the high bias OML law corrected by a dimensionless function G , which takes into account the formation of potential barriers. This function takes values from 0 to 1. Here T_e and T_i are the electron and ion temperature λ_{Di} is the ion Debye length. As shown in Ref. [15], there is a maximum normalized radius of the probe ρ_{max} to operate within the OML regime. Therefore, if $\rho < \rho_{max}$ one has $G = 1$.

For convenience we introduce the following characteristic values

$$I_* \equiv E_m \sigma A, \quad \Phi_* \equiv E_m L^*, \quad \sigma_i \equiv \frac{e E_m L^*}{k T_i} \quad (43)$$

$$L^* \equiv \left(\frac{9\pi^2}{128} \times \frac{1}{G^2(\sigma_i, T_e/T_i, R/\lambda_{Di})} \times \frac{m_e \sigma^2}{e^3} \times \frac{E_m h^2}{N_0^2} \right)^{1/3} \quad (44)$$

with $h \equiv 2A/p$. Note that the definition of σ_i and Eq. 44 yields a nonlinear equation to find L^* . Using the dimensionless variables

$$i \equiv \frac{I}{I_*}, \quad \varphi \equiv \frac{\Phi}{\Phi_*}, \quad \xi \equiv \frac{x}{L^*}, \quad (45)$$

Eq 42 becomes

$$\frac{di}{d\xi} = \frac{3}{4} \frac{G(\sigma_i \varphi, T_e/T_i, R/\lambda_{Di})}{G(\sigma_i, T_e/T_i, R/\lambda_{Di})} \sqrt{\varphi} \quad (46)$$

As shown in Ref. [4], G has a weak dependence on its first argument, which involves the probe bias. This allows us to ignore the G -ratio appearing in the above equation because it

is close to one. One uses the fitting given by Eq. ??, which corresponds to $e\Phi/kT_i = 1000$ without making significative error. This approximation, however, strongly simplifies the problem because it allows to include the *beyond OML effect* inside the parameter L^* . Since $G < 1$ (the collected current is below the OML limit), the characteristic length L^* is enhanced by a factor $G^{-2/3}$

Potential and intensity profiles in the anodic segment is then governed by (Eqs. 41 and 42)

$$\frac{d\varphi}{d\xi} = i - 1 \quad (47)$$

$$\frac{di}{d\xi} = \frac{3}{4}\sqrt{\varphi} \quad (48)$$

and the boundary conditions

$$\xi = 0 \quad \varphi = \varphi_A \quad i = 0 \quad (49)$$

$$\xi = \xi_B \equiv \frac{L_{AB}}{L^*} \quad \varphi = 0, \quad i = i_B \quad (50)$$

For the cathodic segment, $\xi_B < \xi < L/L_* \equiv \xi_L$, the ion current collection can be safely neglected for the deorbiting mode and we write $I(x) \sim I(L_{AB}) \sim I(L)$. The integration of Eq. 41 in this region yields

$$\phi_C = (1 - i_B)(\xi_L - \xi_B) \quad (51)$$

where we introduced the (positive) normalized potential drop $\phi_C \equiv |\Delta V_{HC}|/E_m L_*$.

Figure 3 shows the normalized averaged current versus L/L_* for different hollow cathode potential drops. We remark that the electrodynamic force is proportional to i_{av} (see Eq. 9) and it strongly affects to the performance of the system.

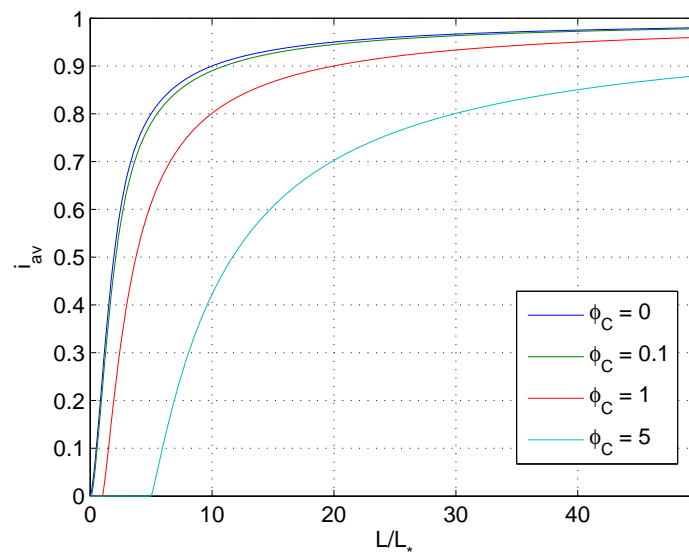


Figure 3: Normalized averaged current versus L/L_* for several hollow cathode potential drops.

0.4.4 Tether survivability model

Tether survivability is a key issue that affects to the design of the mission. BETsMA implements the survivability model presented in Ref. [7] and its optimization algorithm is based on a minimization of the product of the tether-to-satellite mass ratio multiplied by the cut probability [13]. It considers the probability of being cut by a single debris impact with size below one meter. We remark that tethers can maneuver by controlling the hollow-cathode and collisions with large debris can be avoided.

The fatal impact rate per unit length for a tape tether is given by (see Ref. [7] for a detailed explanation)

$$\dot{n}_c \approx -\frac{2}{\pi} \int_0^{\pi/2} d\theta \int_{\delta_{min}}^{\delta_{\infty}} D_{eff}(\delta, \theta) \frac{dF}{d\delta} d\delta \quad (52)$$

where δ is the debris diameter, $F(\delta)$ is the cumulative debris flux,

$$D_{eff}(\delta, \theta) = \delta + W'(\theta) - \delta_{min}(\theta), \quad W'(\theta) = w_t \left(\cos \theta + \frac{h_t}{w_t} \sin \theta \right) \quad (53)$$

and $f_m = 1/3$. The upper limit for the second integral is given by $\delta_{\infty} = 1m$ and the lower limit is

$$\delta_{min} = \begin{cases} f_m W'(\theta) & \theta < \theta^* \\ \delta_{min}^* \equiv \frac{2}{3} \sqrt{\frac{w_t h_t}{\pi}} & \theta > \theta^* \end{cases} \quad (54)$$

where θ^* is the solution of $\delta_{min}^* = f_m W'(\theta^*)$. An integration by parts yields

$$\dot{n}_c \approx -\frac{2}{\pi} \int_0^{\pi/2} \left[D_{eff}(\delta_{\infty}, \theta) F(\delta_{\infty}) - D_{eff}(\delta_m, \theta) F(\delta_m) - \int_{\delta_m(\theta)}^{\delta_{\infty}} F(\delta') d\delta' \right] d\theta \quad (55)$$

BETsMA has data bases of the debris flux as a function of the orbit inclination and altitude, debris size and epoch equal to 2013. They were obtained by using the programs MASTER2005 and ORDEM2000 from ESA and NASA, respectively.

For a given tether geometry, the cut probability N_c is found by solving

$$\frac{dN_c}{dt} = L \dot{n}_c(H, i, w, h) \quad (56)$$

If the user selects the *circular deorbiting model* (the inclination is constant and equal to i_0), BETsMA finds the function $\dot{n}_c(H, i_0)$ as a function of the altitude at the beginning of the simulation. For a non-averaged deorbiting model, BETsMA updates $\dot{n}_c(H, i)$ each time the orbit inclination changes 0.5 degrees.

0.4.5 Growth rate of the dynamical instability and self-balanced tether

As shown in Ref. [11], tethers are affected by a dynamical instability driven by the electrodynamic force. For null current, a tether aligned along the local vertical is a stable steady state. However, for finite current, this equilibrium position is unstable and the tether oscillates. A nonlinear analysis, which assumed a rigid tether, showed that the periodic orbits are unstable with a pumping force proportional to the dimensionless parameter [11, 10, 8, 12]

$$\epsilon_i = \frac{L^2 I_* \mu_m}{I_G \mu} i_{av} \hat{f} \quad (57)$$

where I_G is the moment of inertia relative to a line perpendicular to the tether through its center of mass, $\mu_m = B_{eq} R_E^3$ is the strength of the magnetic dipole and \hat{f} will be defined a few lines below. Following Refs. [10, 8, 12], instead of the mass of the satellite M_s , the mass of the inert and conductive tether segments M_{ci} and the end mass M_B , which includes the deployer, we will use the parameters M_T , ϕ and Λ_t . Here M_T is the total mass $M_T = M_S + M_{ci} + M_B$, $\Lambda_t = M_{ci}/M_T$ and ϕ is given by

$$\cos^2 \phi = \frac{1}{M_T} \left(M_S + \frac{1}{2} M_{ci} \right) \quad (58)$$

$$\sin^2 \phi = \frac{1}{M_T} \left(M_B + \frac{1}{2} M_{ci} \right) \quad (59)$$

Assuming equal density for the inert and conductive tether, one finds

$$I_G = \frac{1}{12} M_T (L + L_i)^2 (3 \sin^2 2\phi - 2\Lambda_t) \quad (60)$$

where L and L_i are the lengths of the conductive and inert tether, respectively. In the particular case $L_i = 0$ and $M_B = 0$ one has

$$I_G = \frac{L^2}{12} m_c \frac{4M_S + m_c}{M_S + m_c} \quad (61)$$

with m_c is the mass of the conductive tether.

The function \hat{f} appearing in Eq. 57 is given by [12]

$$\hat{f} = \cos^2 \phi - f_e \left(\frac{L}{L_*}, \frac{|\Delta V_{HC}|}{E_m I_*} \right) \quad (62)$$

A self-balanced tether satisfies $\hat{f} = 0$ or [12]

$$\cos^2 \phi = f_e \left(\frac{L}{L_*}, \frac{|\Delta V_{HC}|}{E_m I_*} \right) \quad (63)$$

An asymptotic analysis of the stability of the periodic orbits gave the following formula for the growth rate [11]

$$\Gamma \sim \left(\frac{L^2 I_* \mu_m}{I_G \mu} i_{av} \hat{f} \right)^3 \sqrt{\frac{\mu}{a^3}} \cos i \sin^2 i \quad (64)$$

Tether missions should analyze this instability carefully and detailed simulations including flexibility effects must be considered. Probably, a damper or an inert tether segment will be necessary. Such analysis is beyond the scope of BETsMA, which is dedicated to preliminary mission analysis. The parameter Γ should be interpreted as just an indicator of the instability and not a final response to the dynamical instability issue.

0.4.6 Mass estimation of the tether subsystems

The total mass of the tether system is

$$m_T = m_c + m_i + m_{deploy} + m_{HC} + m_{power} \quad (65)$$

where m_c , m_i , m_{deploy} , m_{HC} and m_{power} are the masses of the conductive tether, the inert tether, the deployer, the hollow cathode and the power system, respectively. BETsMA compute the mass of all these components by implementing a set of rules obtained by some of the *BETs* partners. This rules are based on the already developed prototypes.

Figure 4 shows an example of the tether mass calculation. Here the mass of the satellite, the altitude and the inclination are equal to $1000kg$, $1000km$ and 53° , respectively. The geometry of the tether have been chosen without implementing the optimization algorithm.

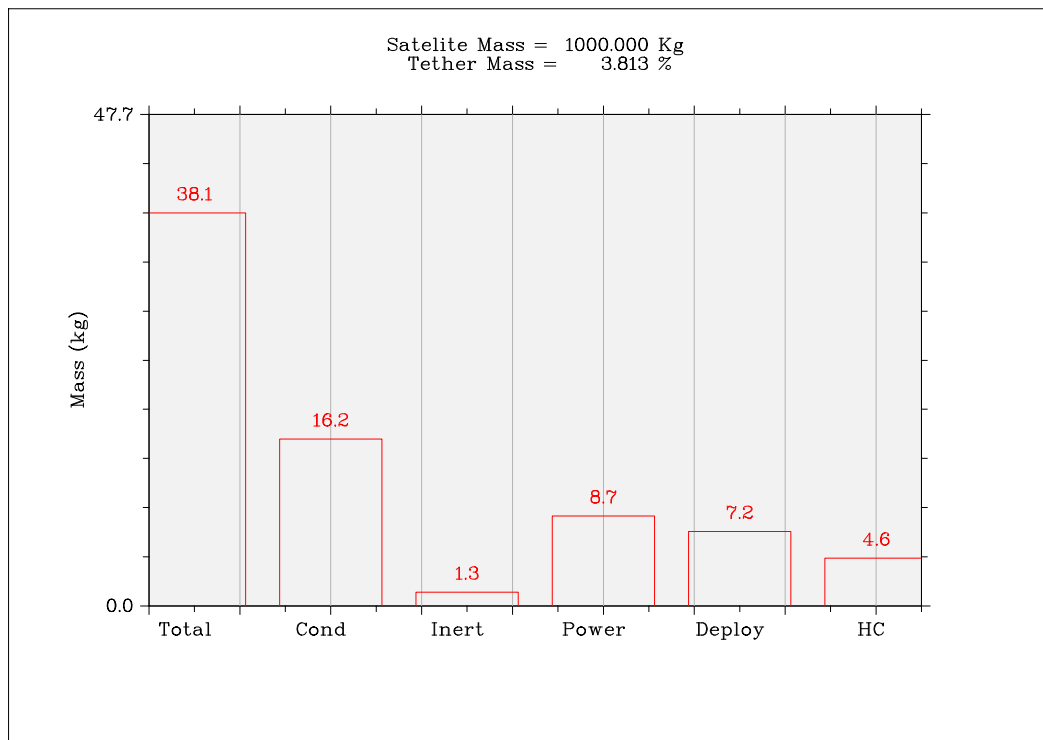


Figure 4: An example of mass calculation. Numbers on the top of the bars indicate the mass in kg units. Tether length, width and thickness is equal to $5km$, $2cm$ and $50\mu m$.

0.5 Optimization method in tape-tether design¹

A well-designed tether mission should satisfy the following requirements:

1. The mass of the conductive tether m_c should be small as compared to the mass of the satellite M_S .
2. The cut probability N_c should be small.
3. The deorbit time should not be too long, i.e. of the order of few months.

Tether geometry, i.e. length L , width w and thickness h , has a deep impact on the above criteria and must be selected correctly. For a given mission, BETsMA *optimization module* helps to find the optimal tether geometry. These values, however, should not be taken as definitive but as a first step for tether design. In addition to the simplifications of BETsMA models (like rigid tether perfectly aligned with the local vertical) one may also take into account other important considerations. For instance, the mass of the subsystems, αm_c with α about 2 – 3, is also affected by tether geometry. On top of this, tape manufacturing or tether deployer manoeuver can also introduce constraints on tether geometry.

BETsMA implements the optimization algorithm presented in Ref. [13], where a detailed description of the target optimization functions is shown.

¹See Ref. [13]

0.6 BETsMA Interface

The user interacts with BETsMA by using the *main* and the *control* windows, which are described in the following lines.

0.6.1 The *main* windows

The *main* window allows to

1. plots the results in the *main* windows (only if DISLIN is included).
2. create a new project, load an old project, save a figure and close BETsMA. When BETsMA is launched, the content of the folder *Projects/Default* is erased and the results of the calculations are written in this folder. If the user want to keep the results of certain calculations, he need to create a new project at the beginning of the computations using the *main* window. This project can be loaded afterwards.
3. see the the version of the code and contact information.

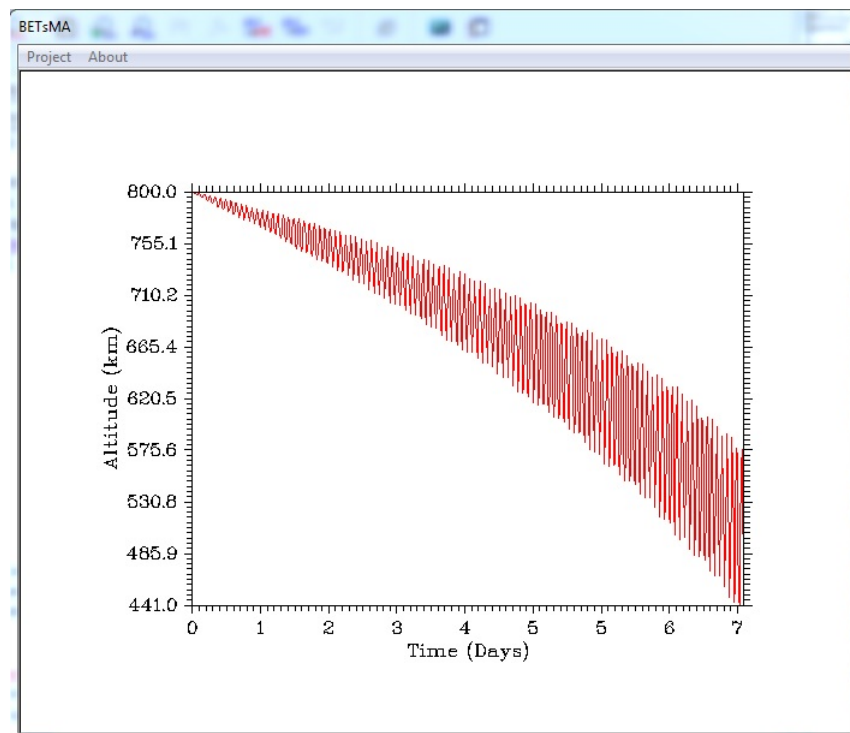


Figure 5: BETsMA main window.

0.6.2 The *control* window

The *control* windows includes the *optimization* and the *deorbiting* modules. Although both tools can be used separately, the user would normally procedure as follows. Given a certain mission, including mass of the satellite and the orbit elements, the *optimization* tool is used to find the tether geometry (width, thickness and length) that minimizes the product of the tether-to-satellite mass ratio by the cut probability. Once the tether geometry is found, a detailed computation of the orbit can be carried with the *deorbiting* tool.

The units and the ranges (in case they exist) of all the input parameters are indicated in the interface (see Fig. 6). If the user try to make a computation with a wrong value of a parameter, the calculation will not be carry out. The user should check the *BETsMA State* dialog box (at the bottom of the *control* window) where error messages and information about the status of the program appear. On the right, the user will find *status bar*, which indicates the progress of the current calculation.

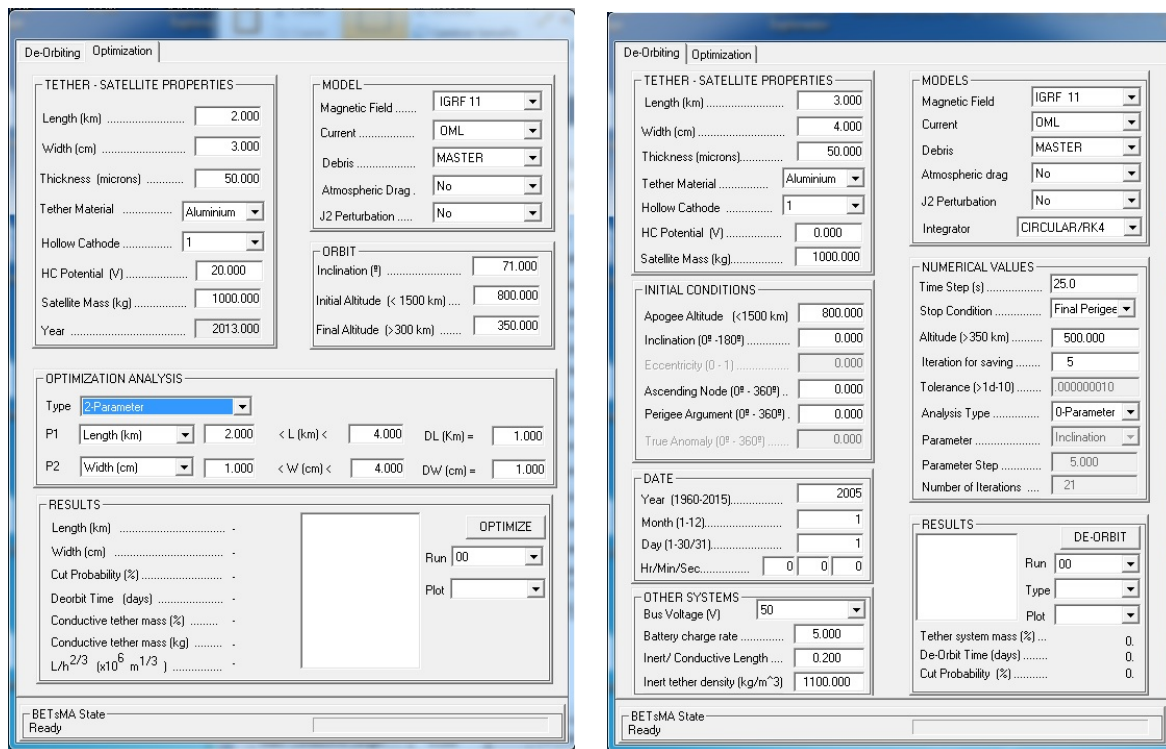


Figure 6: BETsMA optimization (left) and deorbiting (right) user interfaces.

0.6.2.1 The optimization module

The optimization tool has four blocks of input data and a block to control the presentation of the results. They are organized as follows:

1. Tether-Satellite Properties:

- (a) Tether *Length* L (km). Length of the conductive part of the tether.
- (b) Tether *width* w (cm). Width of the conductive part of the tether. BETsMA only considers tape tethers with rectangular section, which are known to be more efficient than round tethers.
- (c) Tether *thickness* h (μm). Thickness of the conductive part of the tether.
- (d) Tether material. Material of the conductive part of the tether. Aluminium has density and conductivity equal to $\rho = 2700$ and $\sigma = 35460000(Ohm\ m)^{-1}$.
- (e) Number of Hollow Cathodes. If the number of hollow cathode is equal to one, No electromagnetic forces will affect the tether during the part of the orbit where the motional electric field points in the wrong direction (a situation that could happen for high inclination orbits).
- (f) Hollow Cathode potential drop (Volts).
- (g) Mass of the host Satellite and the tether system (kg).
- (h) Year of the mission: 2013. BETsMA only has flux data for 2013.

2. Models

- (a) Magnetic field. The Earth magnetic field can be computed by using a simple dipole model, an eccentric dipole model or the IGRF2011.
- (b) Tether current model: short circuit value, OML or beyond OML models.
- (c) Debris flux Model (necessary to compute the cut probability): ESA MASTER model or NASA ORDEM model.
- (d) Atmospheric drag perturbation.
- (e) J_2 zonal harmonic perturbation

3. Orbit:

- (a) Inclination i (deg). This angle is measured from the unit vector \hat{K} to the angular momentum \mathbf{h} and it ranges from 0 to 180° . Orbits with $0 < i < 90$ are direct or prograde orbits and orbits with $90 < i < 180$ are retrograde.
- (b) Initial Altitude (km)
- (c) Final Altitude (km)

4. Optimization Analysis:

- (a) Type of parametric analysis: 0-parameter, 1-parameter or 2-parameter
- (b) First parameter to vary. The user may give the parameter range and the parameter step.

- (c) Second parameter to vary. The user may give the parameter range and the parameter step.

5. Results

- (a) The *optimize* button orders BETsMA to implement the optimization algorithm by using the current values of the interface. The user will see the progress of the computation in the status bar. Each time this button is activated, a folder with the name *Opt_%%* is created inside the folder of the project. The symbol %% denotes the number of the run (these number are chosen consecutively and automatically by BETsMA). Inside the folder *Opt_%%* the user will find two files:
- i. File *F_Optimize.bets*. It contains input parameters of the calculations.
 - ii. File *F_Optim_%%%.dat*. It contains the outputs of the calculations. The % symbol denotes a number. The file *F_Optim_%%%.dat* also contains information about the data organization.
- (b) The *file list box* shows label with the name *Result_%%%* The user can click in the labels to see in the lefthand side of the *Results* frame the result of the calculation. Each number correspond to a different tether geometry.
- (c) The *Run* popup menu allows to explore the content of the folders *Run_%%*. We recall that each time that the *optimize* button is activated a *Run_%%* folder is created.
- (d) The *Plot* popup menu allows to select the type of diagnostic to visualize.
- (e) BETsMA also provides some global values of the computation at the lefthand side of the *Results* frame.

0.6.2.2 The deorbiting module

The deorbiting module includes the following blocks:

1. Tether-Satellite Properties:

- (a) Tether *Length* L (km). Length of the conductive part of the tether.
- (b) Tether *width* w (cm). Width of the conductive part of the tether. BETsMA only considers tape tethers with rectangular section, which are known to be more efficient than round tethers.
- (c) Tether *thickness* h (μm). Thickness of the conductive part of the tether.
- (d) Tether material. Material of the conductive part of the tether. Aluminium has density and conductivity equal to $\rho = 2700$ and $\sigma = 35460000(Ohm\ m)^{-1}$.

- (e) Number of Hollow Cathodes. If the number of hollow cathode is equal to one, No electromagnetic forces will affect the tether during the part of the orbit where the motional electric field points in the wrong direction (a situation that could happen for high inclination orbits).
- (f) Hollow Cathode potential drop (Volts).
- (g) Mass of the host Satellite plus and estimation of the tether system mass (kg).

2. Initial conditions:

- (a) Apogee Altitude r_a (km). This is the maximum altitude during the de-orbiting. Its relation with the major axis a of the initial orbit is $r_a = (1 + e)a$.
- (b) Inclination i (deg). This angle is measured from the unit vector \hat{K} to the angular momentum \mathbf{h} and it ranges from 0 to 180° . Orbits with $0 < i < 90$ are direct or prograde orbits and orbits with $90 < i < 180$ are retrograde.
- (c) Eccentricity e .
- (d) The Right ascension of the ascending node Ω (deg) is the angle in the equatorial plane measured positively from the I axis to the location of the ascending node (point in the equatorial plane where the satellite crosses the equator from south to north). We define \mathbf{n} as the vector with origin the Earth center and pointing to the ascending node.
- (e) Argument of the Perigee ω (deg). Angle between \mathbf{e} and \mathbf{n} . This angle, which varies from 0 to 180° , locates the closest point of the orbit (periapsis).
- (f) True anomaly ν (deg) determines the satellite position relative to the periapsis.

3. Initial Date of the de-orbiting

- (a) Year
- (b) Month
- (c) Day
- (d) Hour/Minutes/Seconds

4. Models

- (a) Magnetic field. The Earth magnetic field can be computed by using a simple dipole model, an eccentric dipole model or the IGRF2011.
- (b) Tether current model: insulated tether, short circuit value, OML or beyond OML models.
- (c) Debris flux Model (necessary to compute the cut probability): ESA MASTER model or NASA ORDEM model.
- (d) Atmospheric drag perturbation.

- (e) J_2 zonal harmonic perturbation
- (f) Integrator. BETsMA integrates the equation of motion with a Runge-Kutta (4 order, fixed time step): averaged circular model or DROMO propagator. The circular integrator automatically set the initial conditions $e = 0$ and $\nu = 0$. For this integrator ω is the angle between the line of nodes and the position vector of the satellite (see initial conditions)

5. Numerical Parameters

- (a) Integration step: Δt (s) for *Circular* or $\Delta\sigma$ for DROMO.
- (b) Stop Condition: perigee altitude or time.
- (c) Final Perigee altitude (>350 km) or final deorbiting time (days). The integration is stopped when one of these conditions is reached. Below $350km$ the aerodynamic drag force is important and the satellite goes down very fast.
- (d) Iteration for saving N_{save} controls the frequency to save the outputs. Outputs will be saved each N_{save} steps.
- (e) Integrator Tolerance: active in future BETsMA version.
- (f) Analysis type can be chosen to 0 – *parameter* (single de-orbiting) or 1 – *parameter* (parameter scan).
- (g) Parameter (only if *Analysis Type* is equal to 1 – *parameter*). Parameter to scan.
- (h) Parameter Step (only if *Analysis Type* is equal to 1 – *parameter*). Increment of the parameter to scan (a positive number).
- (i) Iteration number It_{num} (only if *Analysis Type* is equal to 1 – *parameter*). Number of de-orbiting calculations that will be carry out. Example: if tether length is equal to 2km, Analysis type is equal to 1 – *parameter*, Parameter is equal to *Length*, Parameter step is equal to 0.5 and Iteration number is equal to 5, BETsMA will compute the de-orbiting trajectories for tether lengths equal to 2, 2.5, 3, 3.5 and 4.

6. Other Systems. These values are used to estimate the masses of the different components of the tether-system like the inert tether segment or the power-system.

- (a) Bus voltage (V), used to estimate the mass of the power system.
- (b) Battery charge rate (dimensionless), used to estimate the mass of the power system.
- (c) Ratio L_i/L , with L_i the mass of the inert tether. Electrodynamic tether are affected by a dynamical instability. A portion of inert tether helps to control it.
- (d) Inert tether density. BETs team has considered the PEEK, with density $\rho_i = 1100kg/m^3$.

7. Results

(a) The *deorbit* button orders BETsMA to compute the trajectory of the satellite by using the current values of the interface. The user will see the progress of the integration in the status bar. Each time this button is activated, a folder with the name *Run_%%* is created inside the folder of the project. The symbol %% denotes the number of the run (these number are chosen consecutively and automatically by BETsMA). Inside the folder *Run_%%* the user will find two or three files:

- i. File *F_Deorbiting.bets*. It contains the inputs of the simulation.
- ii. File *F_Orbit_%%%.dat*. It contains the outputs of the simulation. The % symbol denotes a number. If option *Analysis Type* was chosen to *0-parameter*, only the file *F_Orbit_0000.dat* will be created. If option *Analysis Type* was equal to *1-parameter*, the user will find *It_{num}* files of the type *F_Orbit_%%%.dat*, each one with the results of a single orbit. The structure of the *F_Orbit_%%%.dat* is as follows:
 - A. A single number indicating how many orbit points have been saved, N_p .
 - B. N_p rows with 26 columns. Each row contain the following information: [1] Time (s), [2] Semimajor axis (km), [3] eccentricity, [4] inclination (deg), [5] Right ascension of the ascending node (deg), [6] perigee argument (deg), [7] true anomaly (deg), [8] Cut probability, [9] Numerical error (not implemented), [10] Time step (s), [11] Xe mass, [12] altitude (km), [13] dr/dt (m/s), [14] electron density (m^{-3}), [15] Motional electric field E_m (V/m), [16-18] Bx, By and Bz Magnetic field components in the GEI frame (nT), [19] i_{av} , [20] Averaged current along the tether (A), [21] Ion temperature (eV), [22] Electron temperature (eV), [23] Tether Characteristic length L^* (m), [24] air density, [25] OML efficiency, [26] maximum current along the tether (A) and [27] maximum voltage along the tether (V), [28] normalized anodic segment, [29] f_e , [30] Growth rate (1/s)
 - C. A row with 28 columns, including: [1] Satellite mass (Kg), [2] Tether-system mass (kg), [3] Percentage of the tether-system mass, [4] Conductive tether mass (kg), [5] inert tether mass (kg), [6] power-system mass (kg), [7] deployer mass (kg), [8] Hollow-Cathode mass (kg), [9] De-orbit time (s), [10] Maximum current along the tether for the full orbit (A), [11] Total number of cuts for the full orbit, [12] maximum voltage at the anode, [13] altitude variation along the deorbiting, [14] eccentricity variation, [15] inclination variation, [16] Ascending node variation, [17] perigee argument variation, [18] Hollow Cathode dry mass (kg), [19] Hollow Cathode wet mass, [20] Mass of the batteries (kg), [21] Mass of the converter (kg), [22] Mass of the harvester, [23] mass of the power supply (kg), [24] Power dump mass (kg), [25] Power enclosure mass (kg),

[26] Reel mass (kg), [27] Outer Shell mass (kg), [28] Deployer electronic mass (kg).

iii. File *F_Bifurcacion.dat*. This file is created if *Analysis Type* is equal to *1-parameter*. It has It_{num} rows. Each row has 18 column with the following information: [1] Parameter value, [2-18] the last row of the file *F_Orbit_%%%.dat*.

- (b) The *file list box* shows the *F_Orbit_%%%.dat* files and the *F_Bifurcacion.dat* file (if it exist). The user can click in each file to visualize the result of this calculation in the *main* window.
- (c) The *Run* popup menu allows to explore the content of the folders *Run_%%*. We recall that each time that the *deorbit* button is activated a *Run_%%* folder is created.
- (d) The *Type* popup menu allows to select the type of diagnostic to visualize: (i) orbital elements, (ii) Orbit, (iii) Environment, (iv) Electrical, (v) Mass and (vi) Stability.
- (e) The *Plot* popup menu order BETsMA to make a plot in the *main* window. The plot corresponds to the file selected in the *file list box*. Some plot options can produce empty plot; for instance, if the user selects the *OML current model*, the electron and ion plasma temperatures are not necessary for the computation of the orbit and these variables cannot be plot. In case the user selects the *beyond OML current model*, both temperatures are plotted.
- (f) BETsMA also provides some global values of the computation at the bottom of the *Results* frame (for instance the de-orbiting time or the cut of probability). The user can see these values by clicking on the *F_Orbit_%%%.dat* files in the *file list box*.

0.7 Validation of the code

This section summarizes some tests that have been carried out to validate the code. The results are compared with previous works published in the literature or analytical formulas. Each part of the code has been tested in a separated form, including the orbital propagator, the environmental models, the tether survivability model and the optimization tool.

0.7.1 Tether current collection model

The characteristic quantities φ_A , i_B , L_{AB}/L and f_e versus L/L_* for several hollow cathode potential drops computed by BETsMA are shown in Fig. 7.

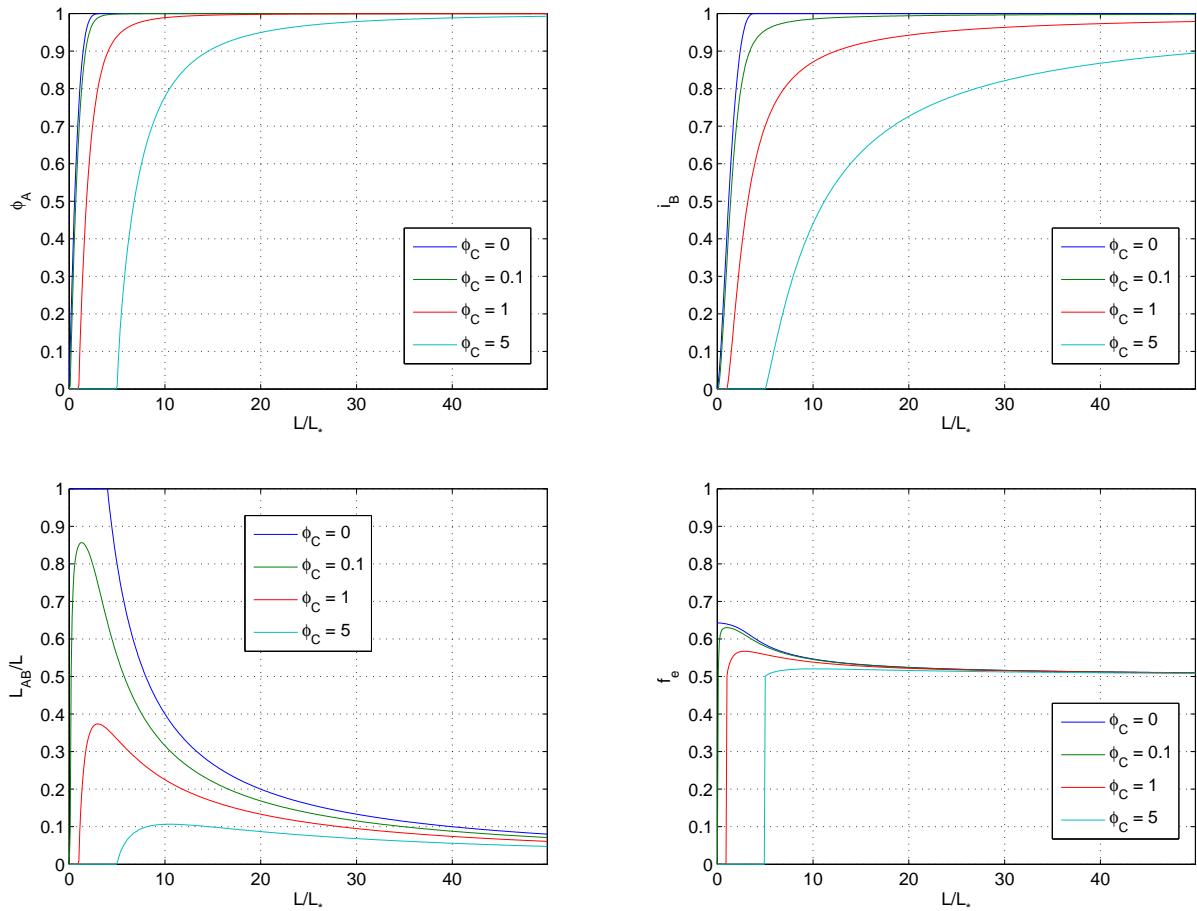


Figure 7: Characteristic magnitudes of the tether current collection versus L/L_* for different hollow cathode potentials.

These results are in agreement with Ref. [1]. The correction of L_* due to the *beyond* OML effect (function $G = I/I_{OML}$) was checked with Refs. [15] and [4].

0.7.2 Tether survival probability

The fatal impact rate per unit length for a tape tether (Eq. 55) is here checked with results from Ref. [6]. Both MASTER and ORDEM flux model are considered. Figure 8 shows \dot{n}_c for a tape tether of width $w = 2cm$ and thickness $h = 50\mu m$ computed with BETsMA. These results are in good agreement with Fig. (5) in Ref. [6].

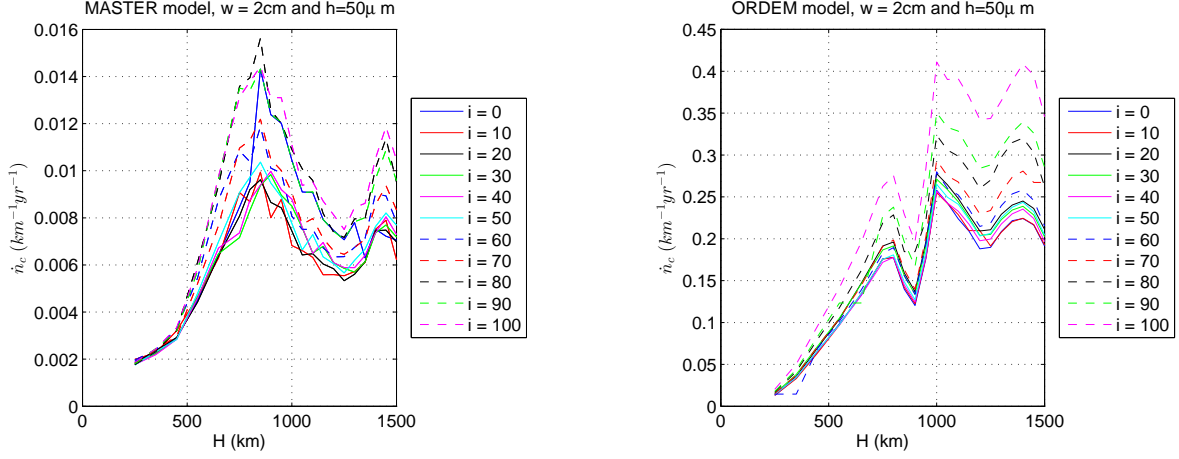


Figure 8: fatal impact rate per unit length for a tape tether of width $w = 2cm$ and thickness $h = 50\mu m$ computed with BETsMA. These results can be compared with Fig. (5) of Ref. [6].

0.7.3 Orbital propagator

The *circular deorbiting model* is almost trivial and its validation has been carried out in Sec. ???. The *non-averaged* deorbiting model (DROMO) has been validated by propagating an orbit perturbed by the J_2 effect. In this case, the secular variation of the orbital parameters are given by

$$\Delta i = \Delta e = \Delta a = 0, \quad (66)$$

$$\frac{d\widehat{\Omega}}{dt} = -\frac{3}{2}J_2 \left(\frac{R_e}{p}\right)^2 n \cos i, \quad \frac{d\widehat{\omega}}{dt} = \frac{3}{4}J_2 \left(\frac{R_e}{p}\right)^2 n (5 \cos^2 i - 1) \quad (67)$$

where $n = \sqrt{\mu/a^3}$.

Figure 9 shows the temporal evolution of an orbit propagated with DROMO. The initial altitude of the apogee, eccentricity and inclinations are equal to $1000km$, 0.04 and 30° . As predicted by the perturbation theory, there is no secular variation of i , e , a and ν . However, the J_2 perturbation produces a secular effect on the longitude of the ascending node Ω and the argument of the perigee ω . Figure 10 displays the secular variation of

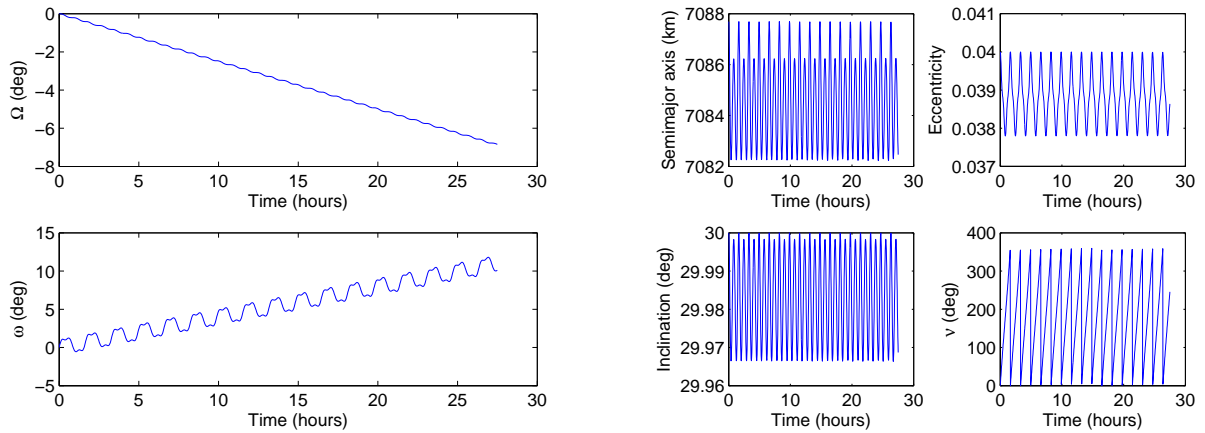


Figure 9: Evolution of the orbital elements computed with DROMO. The satellite perturbed by the J_2 . The initial inclination and eccentricity are equal to 30° and 0.04, respectively.

Ω and ω versus the inclination computed analytically (solid lines) and with *DROMO* (circles). We remark that DROMO set $\Omega = 0$ for equatorial orbits. The agreement with the theoretical prediction is excellent. This results validates the correct implementation of the orbit propagator DROMO in BETsMA.

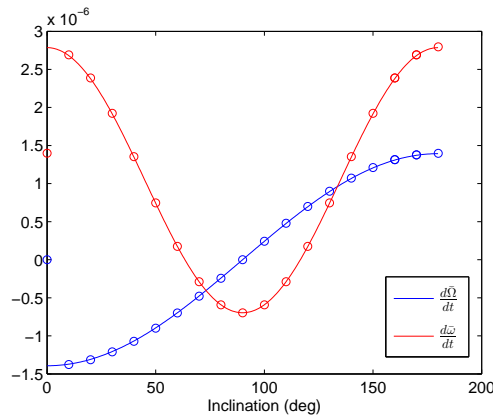


Figure 10: Secular variation of the longitude of the ascending node and the argument of the perigee versus the inclination of the orbit. Solid lines and circles correspond with the results obtained with Eqs. 66 and 67 (perturbation theory) and DROMO.

0.7.4 Global check of the deorbiting module

Individual parts of the subroutines involved in the deorbiting module has been checked by comparing BETsMA results with Dr. Bombardelli's tether flight simulator. The main difference between both simulators is the version of the implemented IRI model. Certain quantities were checked for a single time step, like for instance the Geomagnetic field and the Lorentz force. The results were in agreements.

Figure 11 shows BETsMA deorbit time versus the initial orbit inclination for a 1000 kg satellite equipped with a $3km \times 4cm \times 50\mu m$ tether that operates with 2 hollow cathodes. Initial and final altitudes are equal to 800 and 500 km. Epoch is 2005 and the integration was carried out with DROMO. Bombardelli's simulator provided the values $T_F = 39.2, 146.7, 212.5$ and 127.0 days for inclinations 60, 80, 90, and 100 degrees. Taking into account the differences in the IRI version, results are in reasonable agreement. The comparison of the *circular* integrator with DROMO also showed the expected results.

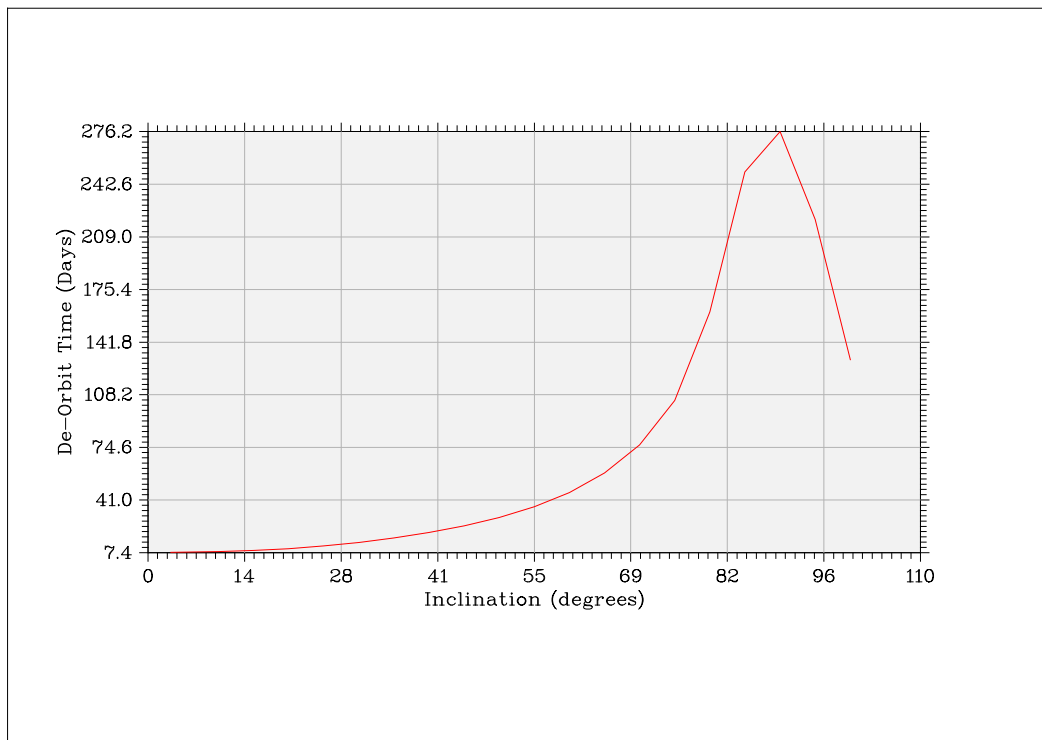


Figure 11: Deorbit time versus the orbit inclination.

0.8 Preliminary mission design example

This section explain how BETsMA can be used to carry out preliminary design of deorbiting missions with bare tethers. Let us consider the input parameter of Table 1. Here, the risk corresponds to the cut probability N_c . For instance, a 3% means that 3 of each 100 missions will have a tether cut. BETsMA provides first number of tether geometry and mission performance. Detailed mission analysis requires an iterative process that involves all tether subsystem and, in particular, dynamical tether simulations including flexibility effects.

Satellite Mass	Apogee Altitude	Inclination	Eccentricity	Year	Risk (N_c)
500 kg	800km	71°	0.005	2013	3%

Table 1: Example of deorbiting mission

0.8.1 Tether optimal geometry

In first place, we use the *optimization module* to find the geometry of the conductive tether segment: length L , width w and thickness h . We recall that the *optimization module* assumes a sequence of circular orbits and works with averaged quantities. In the user interface we set the following values

1. Tether-Satellite Properties
 - (a) Thickness $\rightarrow 50\mu m$
 - (b) Tether Material \rightarrow Aluminium
 - (c) Hollow Cathode $\rightarrow 1$
 - (d) HC Potential $\rightarrow 20V$
 - (e) Satellite Mass $\rightarrow 500kg$
 - (f) Year $\rightarrow 2013$
2. Model
 - (a) Magnetic Field \rightarrow IGRF 11
 - (b) Current \rightarrow OML
 - (c) Debris \rightarrow MASTER
 - (d) Atmospheric Drag \rightarrow No

(e) J_2 Perturbation \rightarrow No

3. Orbit

(a) Inclination $\rightarrow 71^\circ$

(b) Initial Altitude $\rightarrow 800\text{Km}$

(c) Final Altitude $\rightarrow 350\text{Km}$

4. Optimization Analysis

(a) Type \rightarrow 2-parameter

(b) P1 $\rightarrow 0.5\text{Km} < L < 5.5\text{Km}$ and $DL = 0.25\text{km}$

(c) P2 $\rightarrow 0.5\text{cm} < W < 4\text{cm}$ and $DW = 0.25\text{cm}$

Tether length and width in *Tether-Satellite Properties* box are irrelevant because the 2 – parameter option makes BETsMA to vary these two magnitudes. After clicking the button *Optimize*, BETsMA will start the calculations. Once BETsMA finished, the user may plot the product of the cut probability N_c and the conductive tether-to-satellite mass ratio, $\Pi = N_c \times m_c/M_s$, versus the variables $L/h^{2/3}$. This is done by activating the option $N_c m_t/M_s$ in the *Plot* box. Note that BETsMA plots $L/h^{2/3}$ on the top horizontal axis and L in the bottom axis. Using the mouse in the *result list*, different points in the plot can be selected and the tether performance are shown in the *optimization interface*.

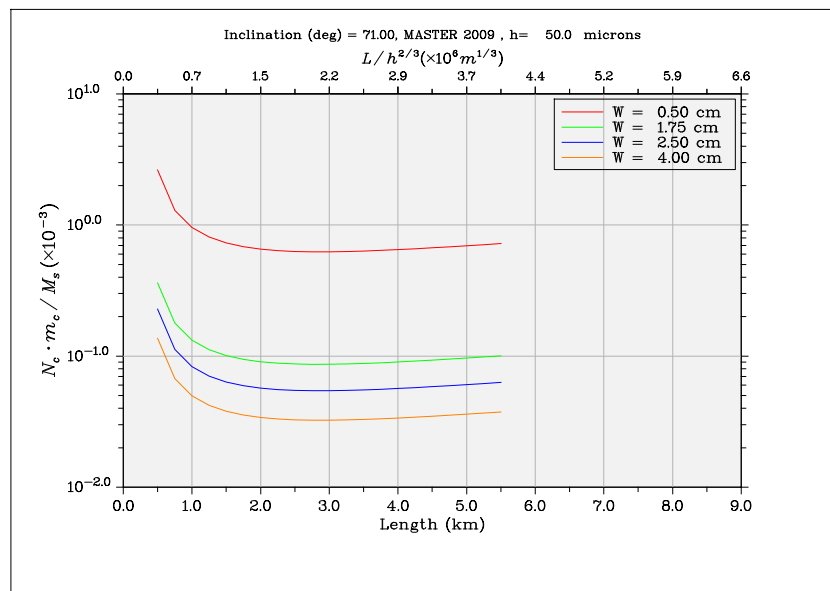


Figure 12: Function Π versus $L/h^{2/3}$ for several tape widths ($h = 50\mu$)

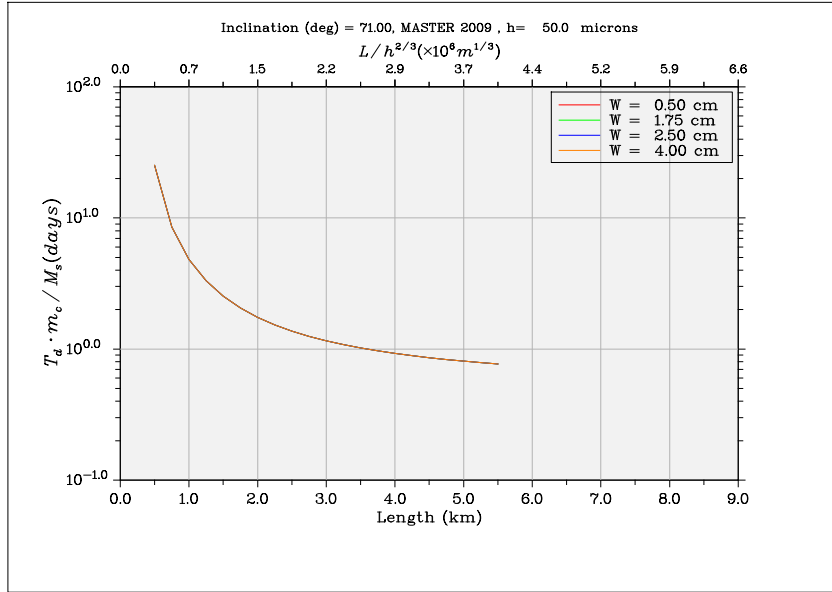


Figure 13: Function $m_c/M_s \times t_d$ versus $L/h^{2/3}$ for several tape widths ($h = 50\mu$)

For this mission, the optimal $L/h^{2/3} |^*$ happens at $2.06 \times 10^6 m^{1/3}$. We now plot (see Fig. 13), which shows the product $m_c/M_s \times t_d$. At the optimal $L/h^{2/3} |^*$, we find $m_c/M_s \times t_d = 1.2482$, thus imposing a constraint on tether performance.

Preliminary conductive tether geometry is chosen by plotting the *Design* diagram in option *Plot*. Fig. 14 shows tether performance (deorbit time, mass ratio and cut probability) versus $L/h^{2/3}$ and w . The intersection of a vertical line at $L/h^{2/3} |^* = 2.06 \times 10^6 m^{1/3}$ with the line $N_c = 3\%$ gives $L = 2.750km$ and $w = 1cm$. At this point one has $m_c/M_s = 0.74\%$ and $T_d = 168$ days. These number are summarized in Table 2. The repetition of this analysis for few tether thickness can provide slightly improved tether performance.

h (μm)	L (km)	w (cm)	T_d (days)	N_c (%)	m_c/M_s (%)
50	2.75	1.0	168	3	0.74

Table 2: Tentative values of tether geometry and performance.

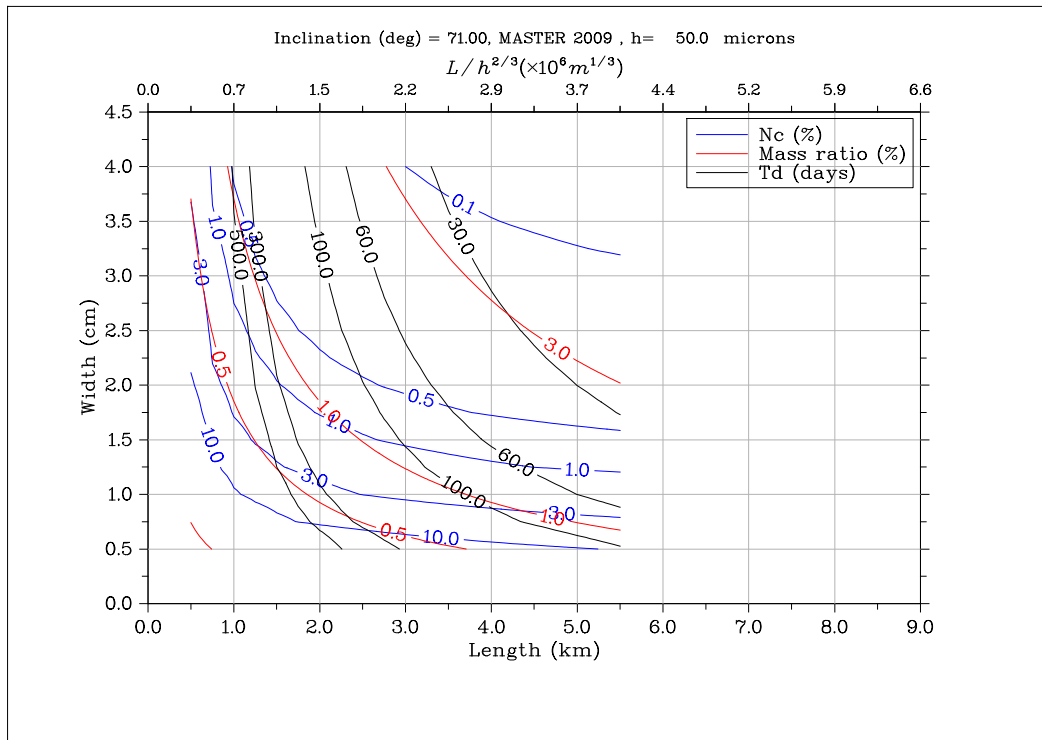


Figure 14: Mission performance versus the conductive tether geomtry ($h = 50\mu$)

0.8.2 Deorbiting mission performance

We now use the *deorbiting module* to simulate the full deorbiting of a mission given by Tables 1 and 2. In the interface we set the same parameters as in the *optimization module* and we add

1. Initial Conditions
 - (a) Eccentricity \rightarrow 0.005
 - (b) Ascending node \rightarrow 0
 - (c) Perigee Argument \rightarrow 0
 - (d) True Anomaly \rightarrow 0
2. Date: Hour/Date \rightarrow 00:00:00, 1/1/2013
3. Numerical Values
 - (a) Integrator \rightarrow DROMO
 - (b) Sigma Step \rightarrow 0.1
 - (c) Stop Condition \rightarrow Final Perigee

- (d) Final Altitude \rightarrow 350km
- (e) Iteration for saving \rightarrow 5
- (f) Analysis Type \rightarrow 0-parameter

4. Other systems

- (a) Bus Voltage \rightarrow 50V
- (b) Battery Charge Rate \rightarrow 5
- (c) Inert/Conductive Length \rightarrow 0.2
- (d) Inert tether density \rightarrow 1100 kg/m^3

Unlike the *optimization module*, DROMO integrator [9] does not assume circular orbit and it does not average the variable over the orbital period; i.e. it computes the trajectories by making a numerical integration of the perturbed Kepler problem. Using the popup menus *Type*, users control the kind of diagnostic to visualize, including orbital elements evolution, environmental variable, electrical tether quantities, mass of the different subsystems and indicator about the tether dynamical instability. For each group of diagnostic, the popup menu *Plot* chooses a particular magnitude. For instance, if tether *electrical* variable is selected, then the *Plot* popup menu can take the following values: motional electric field, L_* , i_{av} , I/I_{OML} , tether current and anode voltage. The selected variable is plotted in BETsMA *main window*.

Table 3 summarizes tether performance computed with the *Deorbiting module*. Note that, thanks to the eccentricity value (0.005), tether performances are better than the one computed with the *Optimization module*, which assumes a quasi-circular deorbiting.

T_d (days)	N_c (%)	m_c/M_s (%)	m_t/M_s (%)	I_{max} (A)	V_{max} (V)
118	1.72	0.74	3.82	1.8	200

Table 3: Tentative values of tether geometry and performance.

Deatiled information about the mission is obtained by exploring the options *Type* and *Plot*. For instance, the evolution of some orbital elements are shown in Fig 15. Fig. 16 displays the maximum and averaged currents as well as the maximum anode voltage. Finally, the masses of the subsystem are shown in Fig. 17.

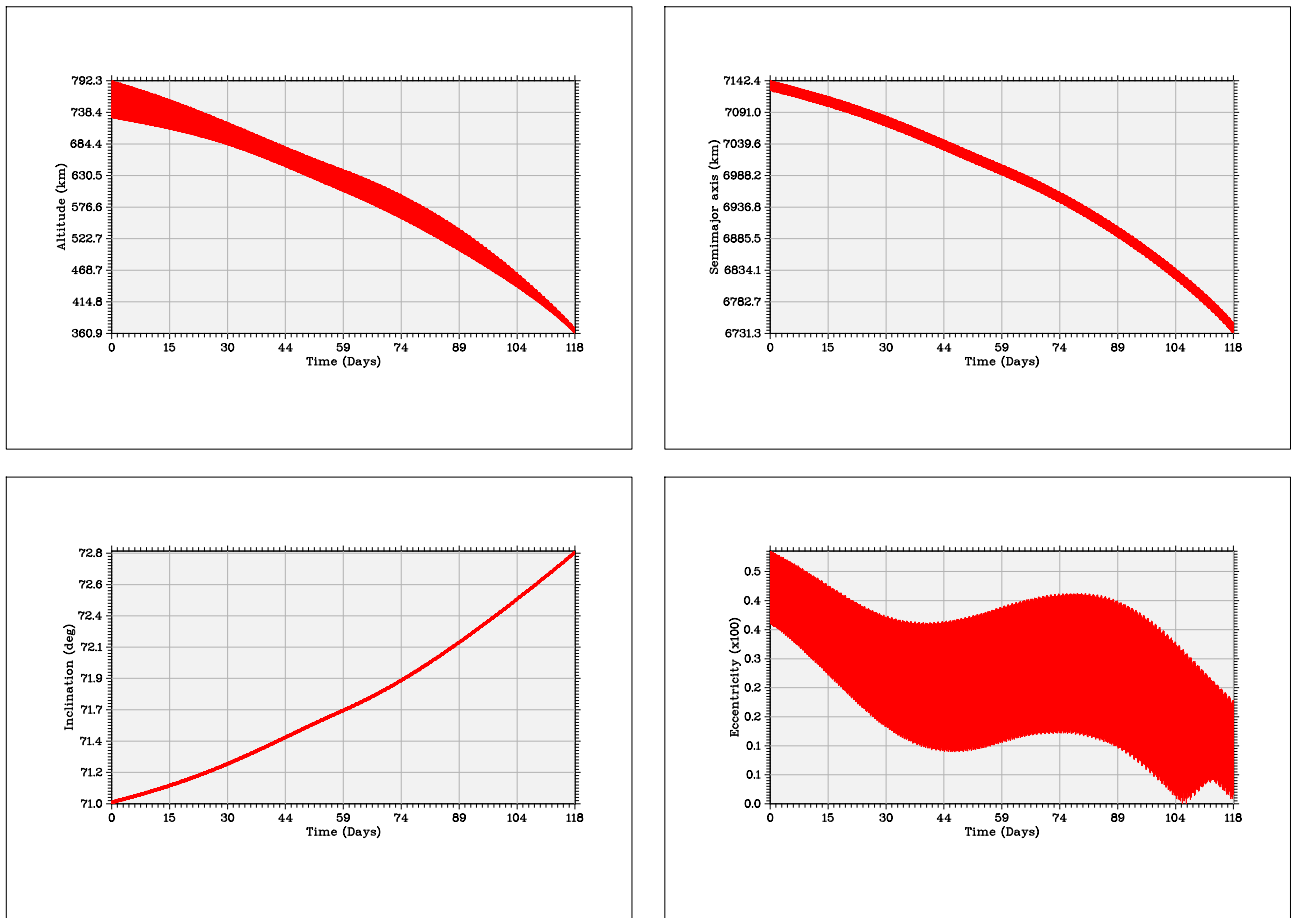


Figure 15: Evolution of orbital parameters computed by the *Orbiting module*

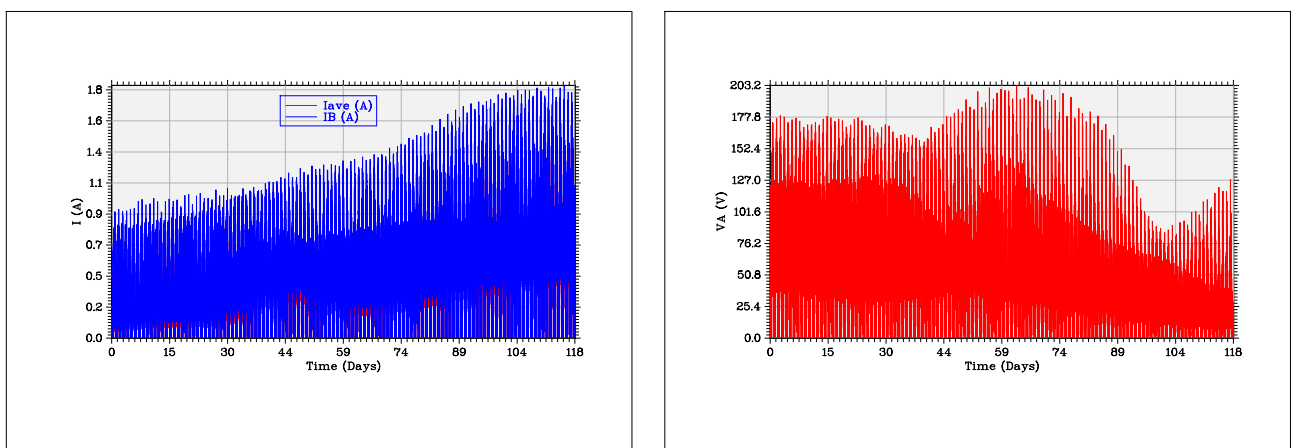


Figure 16: Current and maximum anode voltage versus time

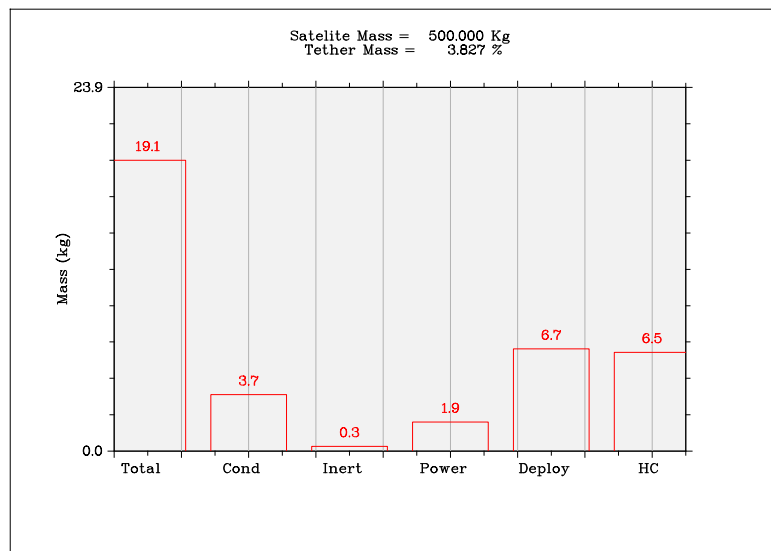


Figure 17: Mass of the tether subsystems.

.1 BETsMA constants

BETsMA uses the physical constant summarized in Table 4.

Variable	Symbol	Value	units
Earth Radius	R_E	6378160	m
Electron mass	m_e	$9.10938291 \times 10^{-31}$	kg
Ion mass	m_i	$1.67262178 \times 10^{-27}$	kg
Electron charge	e	$1.602176565 \times 10^{-19}$	C
Earth gravitational parameter	μ	$398600.436233 \times 10^9$	m^3/s^2
Earth angular velocity	ω_{\oplus}	7.2921158×10^{-5}	rad/s
Earth J_2 zonal harmonic	J_2	1.08265×10^{-3}	-

Table 4: Numerical value of the constants used by BETsMA.

BIBLIOGRAPHY

- [1] E. Ahedo and J. R. Sanmartín. Analysis of Bare-Tether Systems for Deorbiting Low-Earth-Orbit Satellites. *Journal of Spacecraft and Rockets*, 39:198–205, March 2002.
- [2] G. Baù, C. Bombardelli, and J. Peláez. A new set of integrals of motion to propagate the perturbed two-body problem. *Celestial Mechanics and Dynamical Astronomy*, 116:53–78, May 2013.
- [3] D. Bilitza. International reference ionosphere, 2013.
- [4] R. D. Estes and J. R. Sanmartín. Cylindrical Langmuir probes beyond the orbital-motion-limited regime. *Physics of Plasmas*, 7:4320–4325, October 2000.
- [5] C. C. Finlay, S. Maus, C. D. Beggan, T. N. Bondar, A. Chambodut, T. A. Chernova, A. Chulliat, V. P. Golovkov, B. Hamilton, M. Hamoudi, R. Holme, G. Hulot, W. Kuang, B. Langlais, V. Lesur, F. J. Lowes, H. Lühr, S. MacMillan, M. Manda, S. McLean, C. Manoj, M. Menvielle, I. Michaelis, N. Olsen, J. Rauberg, M. Rother, T. J. Sabaka, A. Tangborn, L. Tøffner-Clausen, E. Thébault, A. W. P. Thomson, I. Wardinski, Z. Wei, and T. I. Zvereva. International Geomagnetic Reference Field: the eleventh generation. *Geophysical Journal International*, 183:1216–1230, December 2010.
- [6] S. B. Khan and J. R. Sanmartin. Analysis of tape tether survival in LEO against orbital debris. *Advances in Space Research*.
- [7] S. B. Khan and J. R. Sanmartin. Survival Probability of Round and Tape Tethers Against Debris Impact. *Journal of Spacecraft and Rockets*, 50:603–608, May 2013.
- [8] J. Pelaez and Y. N. Andrés. Dynamic stability of electrodynamic tethers in inclined elliptical orbits. *Journal of Guidance, Control, and dynamics*, 28:611–622, 2005.

- [9] J. Pelaez, J. M. Hedo, and P. R. de Andres. A special perturbation method in orbital dynamics. *Celest. Mech. Dyn. Astron.*, 97, 2007.
- [10] J. Pelaez and M. Lara. Periodic solutions in electrodynamic tethers on inclined orbits. *Journal of Guidance, Control, and dynamics*, 26:395–406, 2003.
- [11] J. Pelaez, E. C. Lorenzini, O. Lopez-Rebollal, and M. Ruiz. A new kind of dynamic instability in electrodynamic tethers. *The Journal of the Astronautical Sciences*, 48:449–476, 2000.
- [12] J. Pelaez and M. Sanjurjo. Generator regime of self-balanced electrodynamic bare tethers. *Journal of Spacecraft and Rockets*, 43:1359–1369, 2005.
- [13] J. Sanmartín, A. Sánchez-Torres, S. B. Khan, and Sánchez-Arriaga G. Tape-Tether design for de-orbiting from given altitude and inclination. *To be submitted*.
- [14] J. R. Sanmartin, E. Ahedo, and M. Martinez-Sanchez. An Anodeless Tether Generator. *Proceedings of Physics of Charged bodies in Space Plasmas*, 1991.
- [15] J. R. Sanmartín and R. D. Estes. The orbital-motion-limited regime of cylindrical Langmuir probes. *Physics of Plasmas*, 6:395–405, January 1999.
- [16] J. R. Sanmartin, M. Martinez-Sanchez, and E. Ahedo. Bare wire anodes for electrodynamic tethers. *Journal of Propulsion and Power*, 9:353–360, June 1993.
- [17] H. Urrutxua, M. Sanjurjo-Rivo, and J. Peláez. DROMO propagator revisited.